Human Molecular Genetics, 2007, Vol. 16, No. 13 ***1604–1618***
doi:10.1093/hmg/ddm110
Advance Access published on May 15, 2007

Mutation of SOD1 in ALS: a gain of a loss of function

Daniela Sau[1,5], Silvia De Biasi[2], Laura Vitellaro-Zuccarello[2], Patrizia Riso[3], Serena Guarnieri[3], Marisa Porrini[3], Silvia Simeoni[1], Valeria Crippa[1,5], Elisa Onesto[1,5], Isabella Palazzolo[1,5], Paola Rusmini[1,5], Elena Bolzoni[1,5], Caterina Bendotti[4] and Angelo Poletti[1,5,*]

[1]Institute of Endocrinology, Center of Excellence on Neurodegenerative Diseases, [2]Department of Biomolecular Sciences and Biotechnologies, [3]Department of Food Science and Microbiology, Division of Human Nutrition, University of Milan, Milan, Italy, [4]Department of Neuroscience, Istituto di Ricerche Farmacologiche Mario Negri, Milan, Italy and [5]InterUniversity Center on Neurodegenerative Diseases of the Universities of Milan, Florence, Rome, Italy

Received October 6, 2006; Revised and Accepted April 25, 2007

Amyotrophic lateral sclerosis (ALS) is a neurodegenerative disease caused by motoneuron loss. Some familial cases (fALS) are linked to mutations of superoxide dismutase type-1 (SOD1), an antioxidant enzyme whose activity is preserved in most mutant forms. Owing to the similarities in sporadic and fALS forms, mutant SOD1 animal and cellular models are a useful tool to study the disease. In transgenic mice expressing either wild-type (wt) human SOD1 or mutant G93A-SOD1, we found that wtSOD1 was present in cytoplasm and in nuclei of motoneurons, whereas mutant SOD1 was mainly cytoplasmic. Similar results were obtained in immortalized motoneurons (NSC34 cells) expressing either wtSOD1 or G93A-SOD1. Analyzing the proteasome activity, responsible for misfolded protein clearance, in the two subcellular compartments, we found proteasome impairment only in the cytoplasm. The effect of G93A-SOD1 exclusion from nuclei was then analyzed after oxidative stress. Cells expressing G93A-SOD1 showed a higher DNA damage compared with those expressing wtSOD1, possibly because of a loss of nuclear protection. The toxicity of mutant SOD1 might, therefore, arise from an initial misfolding (gain of function) reducing nuclear protection from the active enzyme (loss of function in the nuclei), a process that may be involved in ALS pathogenesis.

INTRODUCTION

Amyotrophic lateral sclerosis (ALS) is a fatal neurodegenerative disease characterized by the progressive loss of motoneurons (see 1–3 for a review). Most of the cases are sporadic (sALS), but 10% are familial (fALS) forms inherited in a dominant manner and approximately 20% of these are linked to mutations of Cu/Zn superoxide dismutase type-1 (SOD1), a crucial enzyme for cellular antioxidant defense mechanisms (4). As sALS and SOD1-mediated fALS are clinically indistinguishable and both affect motoneurons with a similar pathology, mutant SOD1 animal and cellular models represent a useful tool to study the disease (1–3). The mutations are thought to confer a gain-of-neurotoxic-function to SOD1 (2); in fact, transgenic mice overexpressing human SOD1 with a glycine to alanine mutation in position 93 (Tg G93A-SOD1 mice) develop an ALS-like phenotype, even in the presence of the endogenous enzyme (5), whereas SOD1 knockout mice do not develop ALS, despite the toxicity of the superoxide radicals (6). However, the exact nature of the toxicity and of the causes of the motoneuronal degeneration is still largely debated (2,3).

The disease-associated mutations are known to destabilize the protein, and compelling data support the notion that fALS should be considered a protein misfolding disorder, in which a non-native toxic oligomeric conformation is generated in the mutant protein(s) (2,3). In fact, there are no hot-spot mutations in SOD1 linked to fALS, suggesting that the whole protein is involved (7,8). Protein misfolding may subsequently trigger a cascade of events which include protein accumulation, possibly followed by axonal transport alterations, mitochondrial and/or proteasome dysfunctions.

*To whom correspondence should be addressed at: Institute of Endocrinology, Center of Excellence on Neurodegenerative Diseases, University of Milan, via Balzaretti 9, 20133 Milan, Italy. Tel: +39 250318215; Fax: +39 250318204; Email: angelo.poletti@unimi.it or angelo.poletti@libero.it

Moreover, these events may indirectly lead to overproduction of reactive oxygen species (ROS) and caspase activation (1–3).

All these events might be intercorrelated, thus exacerbating the severity of the initial trigger, the protein misfolding.

A new intracellular target of SOD1 toxicity has been recently suggested by the finding of neuronal intranuclear protein inclusions, positive for ubiquitin, promyelocytic leukemia gene product and proteasome subunits, reported in an ALS patient (9). Moreover, the levels of 8-hydroxy-2′-deoxyguanosine (8OH2′dG), a well-established marker of oxidative DNA damage, are increased in DNA of sALS patients (10,11), as well as in the spinal cord, frontal cortex and striatum, but not in the cerebellum, of Tg G93A-SOD1 mice (12). Notably, the increased 8OH2′dG levels positively correlate with disease progression (12) and severity (11) (see also 13 for an extensive review).

In this study, we therefore explored the hypothesis that the reduced solubility of mutant G93A-SOD1 may decrease the nuclear protection normally exerted by this enzyme, which is required to block free-radical-induced DNA damage. To this end, we have: (1) analyzed *in vivo* the cellular distribution of SOD1 in transgenic mice expressing either wild-type (wt) or mutant G93A-SOD1; we then further analyzed *in vitro*, in immortalized motoneuronal NSC34 cells, the effects of the G93A-SOD1 mutation (2) on the cytoplasmic and nuclear SOD1 distribution, (3) on SOD1 aggregation and (4) on the proteasome activity in the two subcellular compartments. Finally, (5) we have evaluated the potential nuclear toxicity of SOD1 accumulation.

Collectively, the results show an altered cytoplasmic versus nuclear distribution of mutant G93A-SOD1 compared with wtSOD1 that is not due to an aberrant proteasome function in the two subcellular compartments and that may lead to increased nuclear DNA damage after exposure to oxidative agents.

RESULTS

Immunolocalization of wt and mutant human SOD1 in the spinal cord of transgenic mice

We first analyzed *in vivo* the intracellular distribution of human wt and G93A-SOD1 in lumbar spinal cord sections from transgenic mice expressing either wtSOD1 (Fig. 1A–C) or G93A-SOD1 (Fig. 1D–I) at different disease stages. The two anti-SOD1 antibodies used, a polyclonal recognizing both human and mouse SOD1 (Fig. 1C and F), and a monoclonal specific for human SOD1 (Fig. 1A, B, D, E and G–I), gave comparable results. In wtSOD1 mice, motoneurons always displayed an intense cytoplasmic and nuclear SOD1 labeling at 15 (Fig. 1A) and at 19 weeks of age (Fig. 1B and C). The distribution of mutant G93A-SOD1 was instead markedly different because both at 15 (Fig. 1D) and at 19 weeks of age (Fig. 1F–H) the vast majority of motoneurons in Tg G93A-SOD1 mice showed an intense and diffuse SOD1 labeling confined to the cytoplasm, leaving the nucleus unstained. In end-stage animals, cytoplasmic G93A-SOD1 labeling was typically present in numerous vacuolated motoneurons (Fig. 1E, H, H′) and in the rim of several vacuolated profiles scattered in the neuropil of the ventral horn (Fig. 1G), as previously described (14–16). Only occasionally, G93A-SOD1 labeling was found in the nucleus of morphologically intact motoneurons lacking cytoplasmic vacuoles (Fig. 1E). Interestingly, also in pre-symptomatic 6-week-old Tg G93A-SOD1 mice, vacuolated motoneurons showed exclusively a cytoplasmic SOD1 labeling (Fig. 1I). These findings suggest that the biochemical properties of the G93A-SOD1 are modified with respect to those of the wtSOD1 and, as a consequence, the mutant enzyme is excluded from the nucleus.

Localization of wt and mutant human SOD1 expressed in NSC34 cells

To better characterize the effects of the G93A-SOD1 mutation, we used a cellular model of fALS. The model consists of immortalized motoneurons, the NSC34 cells, that are an hybrid cell line obtained from mouse motoneuron-enriched spinal cord cells fused with mouse neuroblastoma cells (17,18). These cells, which display a multipolar neuronal-like aspect (Fig. 2A) and whose motoneuronal phenotype has been fully characterized (17,18), are routinely used in our laboratory (19–22) as a model for an ALS-related motoneuron disease known as spinal and bulbar muscular atrophy (23,24). In this study, we have transfected NSC34 cells with plasmids encoding either the wtSOD1 or the G93A-SOD1, subsequently detected by immunocytochemistry.

The results show that in most of the NSC34 cells transfected with wtSOD1, the immunoreactivity for SOD1 is mainly diffusely localized in perikarya and neurites but it is also present in the nuclear compartment (Fig. 2B and C). In our experimental conditions, the fluorescence detected in transiently transfected cells is only due to the immunoreactivity of the human SOD1, because a very low signal of the endogenous mouse SOD1 was detectable in untransfected cells (compare the cell marked with the asterisk in Fig. 2A and B). In all the experiments, we never found SOD1 aggregates in wtSOD1 expressing cells. Conversely, NSC34 cells transfected with mutant G93A-SOD1 showed a more reticular perikaryal distribution of the protein (Fig. 2D–F) and occasional neuritic swellings enriched in G93A-SOD1 (Fig. 2D). In the cell body, cytoplasmic aggregates of SOD1 were often present (Fig. 2E and Table 1), but a large amount of G93A-SOD1 remained unsequestered (diffuse) and largely concentrated in the perinuclear region. Most of the nuclei were devoid of G93A-SOD1 (Fig. 2D–F), however, when G93A-SOD1 was present in the nucleus, it was fully segregated into aggregates (Fig. 2F, arrows). The intranuclear localization of aggregates containing G93A-SOD1 immunoreactivity is clearly demonstrated in series of confocal images taken at 1 μm intervals through the *z*-axis of NSC34 cells (Fig. 2, G_1–G_9) and in the relative projection (Fig. 2, G_0).

To confirm that the wtSOD1 may also localize into the nucleus whereas the mutant SOD1 is generally excluded from this compartment, we analyzed the intracellular distribution of wt and mutant SOD1s in living cells, using fluorescent-tagged SOD1. To better distinguish the cytoplasmic versus the nuclear localization, we also used chimeric fluorescent-tagged proteins bearing either a nuclear export signal (NES) or a nuclear localization signal (NLS). The results are reported in Fig. 2H–O. The CyanFP (CFP)-tagged wtSOD1 is distributed both in the cytoplasm and in the nucleus

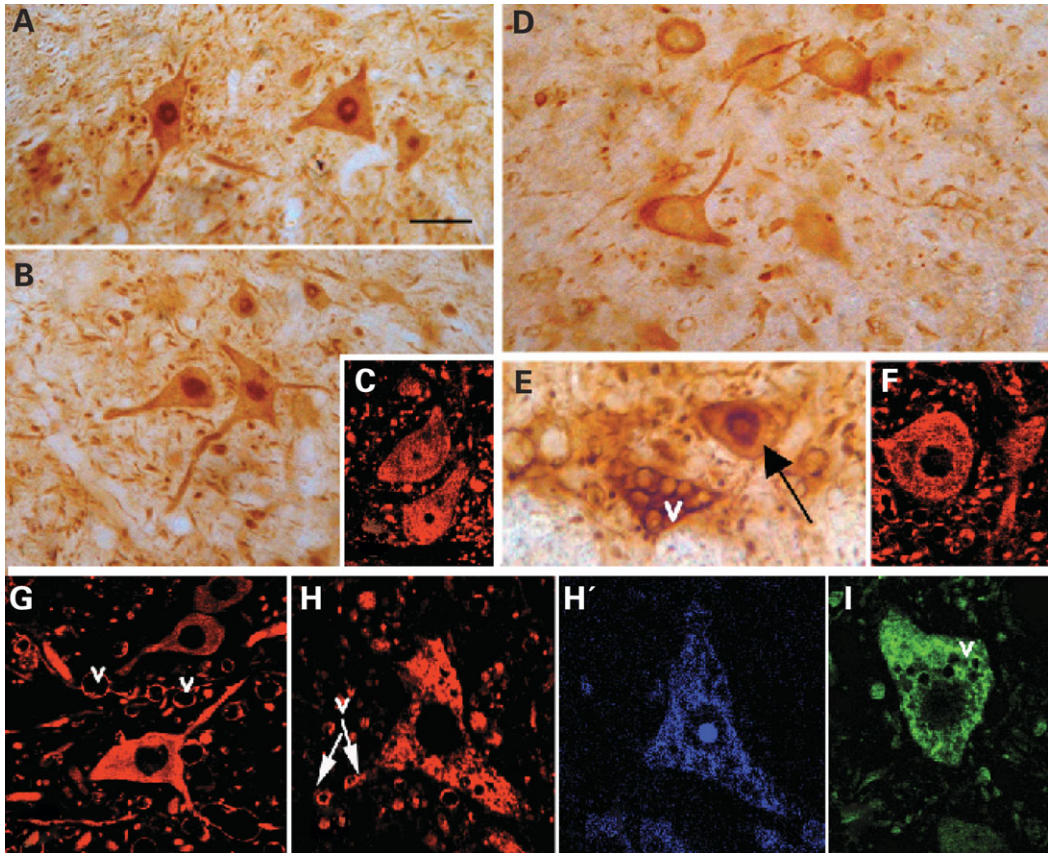

Figure 1. Immunocytochemical localization of human SOD1 in vibratome spinal cord sections from transgenic wtSOD1 mice and from Tg G93A-SOD1 mice. The analysis was performed using a polyclonal anti-SOD1 antiserum (**C**, **F**) or a monoclonal anti-human SOD1 antibody (**A**, **B**, **D**, **E**, **G**–**I**). In wtSOD1 mice at 15 weeks (A) and at 19 weeks (B and C), motor neurons always show intense cytoplasmic and nuclear SOD1 labeling. In G93A-SOD1 mice at 15 weeks (D) and 19 weeks (E–H′), motor neurons show an intense and diffuse cytoplasmic SOD1 labeling; the nucleus is unstained both in morphologically intact motor neurons (D, F, G) and in vacuolated (H) motor neurons. Only occasionally (E) SOD1 labeling is present in the nucleus of morphologically intact motor neurons (arrow) close to vacuolated neurons (v). (G) Several vacuolated profiles (v) with an SOD1-positive rim are scattered in the neuropil surrounding morphologically intact motor neurons. (H–H′) A vacuolated SOD1-positive motor neuron with cytoplasmic SOD1 labeling excluded from the nucleus (H) counterstained with NeuroTrace (H′) to reveal Nissl substance and nucleolus. (I) Vacuolated motor neuron with cytoplasmic SOD1 labeling excluded from the nucleus in a presymptomatic 6-week-old G93A-SOD1 mice. (A, B, D and E) Light micrographs from vibratome sections stained with a DAB-based immunoperoxidase method. (C, F, G–I) Confocal images from vibratome sections stained with an immunofluorescence method. Scale bars: A–D, 30 μm; E and G, 27 μm; H and F, 20 μm; I, 16 μm.

(Fig. 2H), as seen in immunocytochemistry with the untagged SOD1 (Fig. 2B and C). The insertion of a NES in the YellowFP (YFP)-wtSOD1 completely prevented the appearance of fluorescence in the nuclei (Fig. 2I), thus supporting the evidence that the nuclear fluorescence observed in Fig. 2C and H is due to the nuclear localization of wtSOD1. The NLS inserted as a control in the YFP-wtSOD1 induced an almost complete nuclear segregation of SOD1 (Fig. 2L). The CFP-G93A-SOD1 localized mainly in the cytoplasm (Fig. 2M), as seen in immunocytochemistry with the untagged G93A-SOD1 (Fig. 2D–F). The insertion of the NES did not change the fluorescence pattern (Fig. 2N) or the aggregation rate (not shown) observed in transfected cells, whereas the insertion of the NLS resulted in a complete nuclear localization of the mutant SOD1 (Fig. 2O). In these conditions, it was not possible to estimate the number of nuclear aggregates due to the presence of significant amounts of diffuse fluorescent protein. Interestingly, no cytoplasmic aggregates were detectable using this chimeric protein.

We have statistically analyzed the differences in cytoplasmic versus nuclear SOD1 immunoreactivity considering, for technical reasons, only the cells devoid of cytoplasmic or nuclear aggregates (Table 1). Although both wt and G93A-SOD1s were mainly localized in the perikarya, considerable amounts of wtSOD1 immunoreactivity were detectable also in the nuclei. The average cytoplasmic levels of wt and G93A-SOD1s were comparable, whereas the average nuclear levels of the two SOD1 forms significantly differed, with a massive reduction (about 2-fold) of the G93A-SOD1 compared with the wtSOD1. By estimating, in each single cell, the ratio between nuclear and cytoplasmic fluorescence, we found a robust decrease ($P < 0.0001$) of the intranuclear G93A-SOD1 protein with respect to the wtSOD1.

We have also statistically analyzed the number and distribution of SOD1 intracellular aggregates (Tables 2 and 3). Approximately 40% of the transfected cells displayed SOD1-positive aggregates. Of these, more than 50% contained perikaryal aggregates (1.1 aggregates per cell), and almost 40%

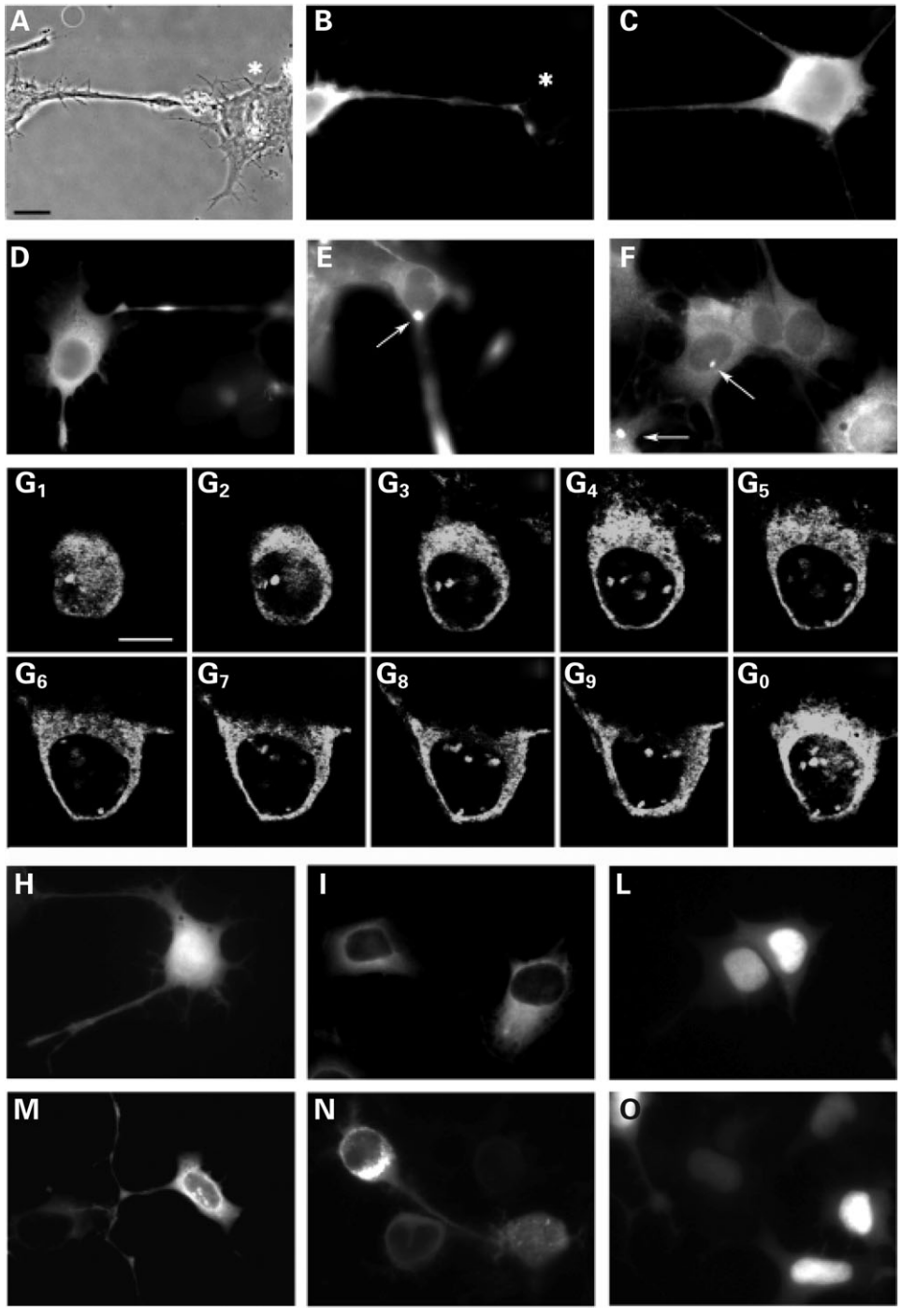

Figure 2. Localization of wt and mutant SOD1s expressed in immortalized motoneuron NSC34 cells. Immunofluorescence analysis performed on immortalized motoneurons (NSC34) transfected with wt (**B**, **C**) or G93A-SOD1 (**D**–**F**), using a polyclonal anti-SOD1 antiserum. (**A**) Phase contrast of NSC34 cells transfected with human wtSOD1. The human SOD1 immunoreactive cells are shown in (B); the cell labeled with the asterisk demonstrates that a very low fluorescent signal is present in untransfected cells expressing the endogenous mouse SOD1. (B and C) Diffused distribution of wtSOD1 in perikarya, neurites and nuclei. (D–F) Nuclear exclusion and reticular perikaryal distribution in NSC34 cells expressing mutant G93A-SOD1 with occasional neuritic swellings enriched of SOD1 immunoreactivity (D). (E and F) Cytoplasmic aggregates of segregated mutant G93A-SOD1 in the cell body and nuclei, respectively (arrows). Confocal single optical sections about 1 μm thick, taken at 1 μm intervals through the *z*-axis (G_1–G_9) and projection (G_0) of an NSC34 cell transfected with G93A-SOD1 and immunolabeled with anti-SOD1. Besides the cytoplasmic SOD1 labeling, several SOD1-positive aggregates are evident throughout the nucleus. Scale bar: 10 μm. (**H**–**O**) Fluorescence microscopy on NSC34 cells expressing chimeric fluorescent-tagged SOD1s proteins. (H) CFP-tagged wtSOD1 (CFP-wtSOD1); (I) YFP-tagged wtSOD1 targeted to the cytoplasm using a nuclear export signal (YFP-NES-wtSOD1); (L) YFP-tagged wtSOD1 targeted to the nucleus using a nuclear localization signal (YFP-NLS-wtSOD1); (M) CFP-tagged G93A-SOD1 (CFP-G93A-SOD1); (N) YFP-tagged G93A-SOD1 targeted to the cytoplasm using a nuclear export signal (YFP-NES-G93A-SOD1); (O) YFP-tagged G93A-SOD1 targeted to the nucleus using a nuclear localization signal (YFP-NLS-G93A-SOD1).

Table 1. Cytoplasmic versus nuclear wt and mutant SOD1

	wtSOD1	G93A-SOD1
Cytoplasmic integrated intensity	3.68 ± 0.03	3.34 ± 0.042
Unclear integrated intensity	2.31 ± 0.02	1.18 ± 0.02[a]
Nuclear/cytoplasmic intensity ratio[b]	0.67 ± 0.22	0.36 ± 0.10[c]

Gray levels sum/region area.
[a]$P < 0.0001$ versus *nuclear wtSOD1*.
[b]Average of the intensity ratios obtained from each single-cell assay.
[c]$P < 0.0001$ versus *wtSOD1*.

Table 2. G93A-SOD1 aggregates on total transfected cells

	Means ± SD
% Cell with aggregates on total transfected cells	41.79 ± 11.06

Table 3. G93A-SOD1 subcellular aggregate ratio

	Mean ± SD
Cytoplasmic aggregates	
% Cell with aggregates	53.41 ± 24.13
Number aggregates/cells	1.10 ± 0.14
Nuclear aggregates	
% Cell with aggregates	37.71 ± 14.62
Number aggregates/cells	1.20 ± 0.30
Cytoplasmic and nuclear aggregates	
% Cell with both type of aggregates	8.90 ± 5.45

contained nuclear aggregates (1.2 aggregates per cell). Approximately 9% of the aggregate-containing cells displayed SOD1 aggregates in both compartments. Altogether, this peculiar distribution of SOD1 aggregates suggests that the mechanisms of their formation might be very selective.

Biochemical features of wt and mutant human SOD1 expressed in NSC34 cells

Some biochemical features of SOD1s expressed in immortalized motoneurons are shown in Fig. 3A and B. Filter retardation assays (Fig. 3A) performed (22,25) using cell lysates of NSC34 cells expressing wt or G93A-SOD1 demonstrate that wtSOD1 is not retained by the cellulose acetate membranes, either in the absence or in the presence of the proteasome inhibitor MG132. Therefore, wtSOD1 remains soluble even during proteasome impairment. Conversely, significant amounts of insoluble G93A-SOD1 were detectable even in basal conditions ($P < 0.01$ versus wtSOD1 ± MG132), suggesting that G93A-SOD1 generates misfolded species that are capable to produce aggregates. When proteasome activity was impaired with MG132, there was an exponential increase ($P < 0.01$ versus untreated G93A-SOD1) of insoluble G93A-SOD1. This observation may be relevant to understand the molecular mechanisms involved in ALS. Very low intracellular levels of insoluble proteins are in fact expected with a functional proteasome, whereas an increase in the accumulation rate of G93A-SOD1 is predicted to perturb (temporarily or continuously) the proteasome activity.

A representative western blot of immortalized motoneurons expressing wt or G93A-SOD1 is shown in Fig. 3B. The G93A-SOD1 levels are normally lower than those obtained in the same conditions using the wtSOD1. Occasionally, high-molecular-weight species of SOD1 (indicated as SOD1 oligomers) (26) were detectable; sporadically, sodium dodecyl sulfate (SDS)-resistant forms were also observed in the stacking gels (not shown) only in G93A-SOD1 samples, suggesting that PBS-insoluble forms of G93A-SOD1 detected in filter retardation assay may evolve into SDS-resistant species.

Effects of wt and mutant human SOD1 expressed in NSC34 cells on the proteasome

We have then analyzed whether wtSOD1 and/or G93A-SOD1 alter proteasome functions using the YFPu reporter system (22). YFPu derives from GFPu (27,28) and consists of a short degron (CL1) signal for the ubiquitin-proteasome pathway fused to the YFP C-terminus (22). YFPu is rapidly degraded by the proteasome, but accumulates in cells when the proteasome is impaired. Fig. 3B (middle inset) shows the effects of the two SOD1s on proteasome activity. The YFPu is fully degraded in NSC34 cells expressing wtSOD1, but it accumulates, as expected, if the cells are treated with MG132. Conversely, YFPu accumulates at very high levels in NSC34 cells expressing G93A-SOD1 and in these cells the proteasome saturation generated by the mutant SOD1 is even higher than that obtained with MG132 on cells expressing wtSOD1. Interestingly, a robust additive effect is present when the treatment with the proteasome inhibitor is performed on NSC34 cells expressing the G93A-SOD1, suggesting that the two mechanisms cooperate to impair the proteasome.

Effects of wt and mutant human SOD1 expressed in NSC34 cells on cytoplasmic or nuclear proteasome

On the basis of the two intriguing observations reported, i.e. the different subcellular concentration and aggregation of G93A-SOD1 versus wtSOD1, and the effect of G93A-SOD1 on the proteasome, we further investigated whether the lack of nuclear G93A-SOD1 could be due to increased protein processing by nuclear proteasome. We have initially evaluated whether the alteration of G93A-SOD1 distribution was associated with changes in protein concentrations (rather than with epitope availability in intact cells). Western blot analysis confirmed the presence of wtSOD1 in the nuclei (Fig. 4A), as well as the reduction of the relative amount of nuclear G93A-SOD1 compared with nuclear wtSOD1 (Sp1 was used to test the nuclear preparations obtained using the NE-PER kit). Only marginal differences are observed in the cytoplasm (see also Fig. 3B showing the total intracellular levels of SOD1s). In fact, the optical density analysis of the immunoreactive SOD1 bands (Fig. 4B) shows no significant differences between cytoplasmic wtSOD1 and G93A-SOD1s levels (means ± SD

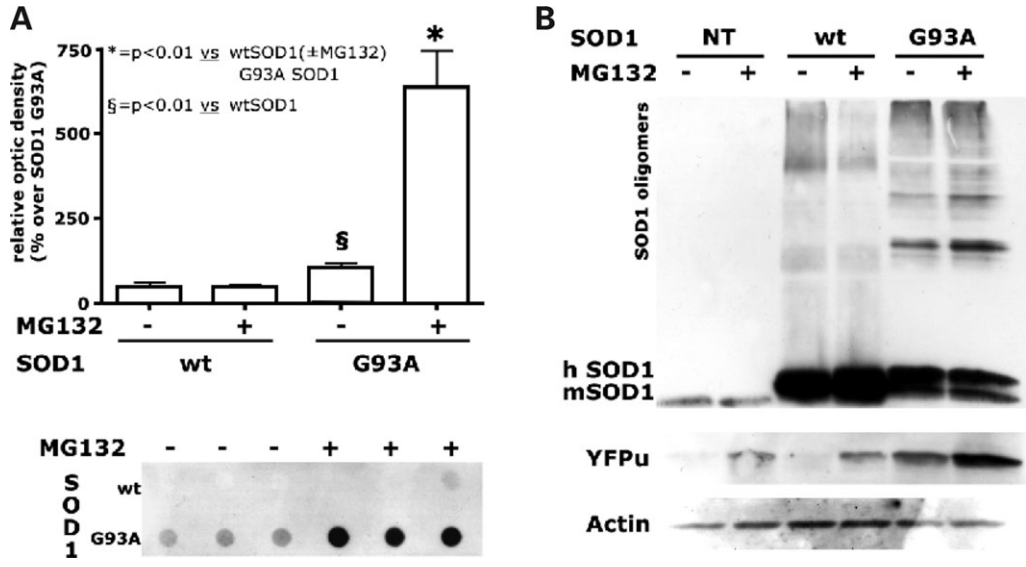

Figure 3. Biochemical properties of wt and mutant SOD1s expressed in immortalized motoneuron NSC34 cells. (**A**) Filter retardation assays (see Materials an Methods), performed on NSC34 transfected with wt and mutant G93A-SOD1 in the presence or in the absence of the proteasome inhibitor MG132. The histogram in the upper inset has been obtained from the optical densities of the spots measured in experiments performed in triplicate; the wtSOD1 is not retained by the cellulose acetate membranes even in MG132. A typical filter retardation assay, showing that significant amount of insoluble species of G93A-SOD1 (exponential increased with MG132) are detectable ($P < 0.01$ versus wtSOD1 $\pm$ MG132) in NSC34-transfected cell lysates, is reported in the lower inset ($P < 0.01$ versus untreated G93A-SOD1). (**B**) Western blot assay performed using the polyclonal anti-SOD1 antibody (upper inset, see Materials an Methods) on cell lysates of NSC34 transfected with the proteasome reporter YFPu and either wt or mutant G93A-SOD1. The analyses have been performed in the presence or in the absence of the proteasome inhibitor MG132. hSOD1 indicates the transfected human SOD1 monomeric forms; mSOD indicates endogenous mouse SOD1. SOD1 oligomers indicate the presence of dimeric and high-molecular oligomeric species of human SOD1; these forms were detectable only in samples expressing mutant G93A-SOD1. Accumulation of the proteasome reporter YFPu was detected on the same blot using a monoclonal anti-GFP antibody (middle inset, see Materials and Methods). Equal protein loading was assayed by evaluating total actin using a polyclonal anti-actin antibody (lower inset, see Materials and Methods) as a control.

from nine independent experiments). In the nucleus, the concentration of wtSOD1 was significantly lower than in the cytoplasm ($P < 0.01$), confirming however that, besides its main cytoplasmic localization (see Table 1), wtSOD1 may also enter into nucleus. The nuclear G93A-SOD1 levels were significantly lower ($P < 0.0001$) than the nuclear wtSOD1 levels and clearly also of the levels of both cytoplasmic SOD1s forms. The endogenous murine SOD1 is also detectable in the nuclear fraction, even if at lower levels than those observed for the transfected human wtSOD1; this is because of the fact that exposure time was optimized to detect the recombinant overexpressed protein. In cells expressing the G93A-SOD1, the nuclear levels of the endogenous murine SOD1 are further reduced; this observation may be explained by its sequestration into the insoluble species formed by the mutant SOD1, as already shown by Deng *et al*. (29).

In preparations of nuclei, we also analyzed the presence of SOD1 immunoreactivity in comparison with DAPI staining. Unfortunately, in the samples obtained with the commercially distributed nuclear and cytoplasmic extraction reagent (NE-PER, see Materials and Methods), we were unable to identify the cells transfected with the mutant SOD1, as this protein is excluded from the nucleus. To this purpose and for this assay, we adopted a milder procedure to purify the nuclei (see Materials and Methods) that allows to retain a portion of cytoplasm surrounding the nucleus and therefore to identify the cells transfected with the mutant SOD1. The results indicate that the wtSOD1 immunoreactivity colocalizes with DAPI staining, whereas the G93A-SOD1 immunoreactivity never does, even in the presence of cytoplasmic residues, thus confirming that the nuclei of cells expressing the mutant SOD1 do not contain the enzyme (Fig. 4C).

The exclusion of the mutant SOD1 from the nuclei may be due either to the formation of high MW species, unable to diffuse through the nuclear membrane, or to an increased nuclear degradation of the aberrant protein. In the second case, the G93A-SOD1 misfolding may be exacerbated by the nuclear environment, leading to a faster degradation by the proteasome. We thus modified the YFPu protein by adding either a NES (from the cAMP-dependent protein kinase inhibitor) or a NLS (from the large T antigen of the SV40), to selectively measure the proteasome activities in the two compartments under the experimental conditions cited above (22). We have already shown that in NSC34 cells expressing YFPu_NES or YFPu_NLS, both proteasome reporters accumulated in a dose-dependent manner in the presence of increasing concentrations of MG132 (up to 100 μM) (22). Fig. 4D recapitulates the results obtained using YFPu_NES or YFPu_NLS. The western blot on the left, performed on NSC34 cells transfected with the YFPu_NES and either wtSOD1 or G93A-SOD1 to measure cytoplasmic proteasome activity, shows that no detectable amounts of YFPu_NES were present with wtSOD1 in the absence of MG132, whereas a marked YFPu_NES accumulation was

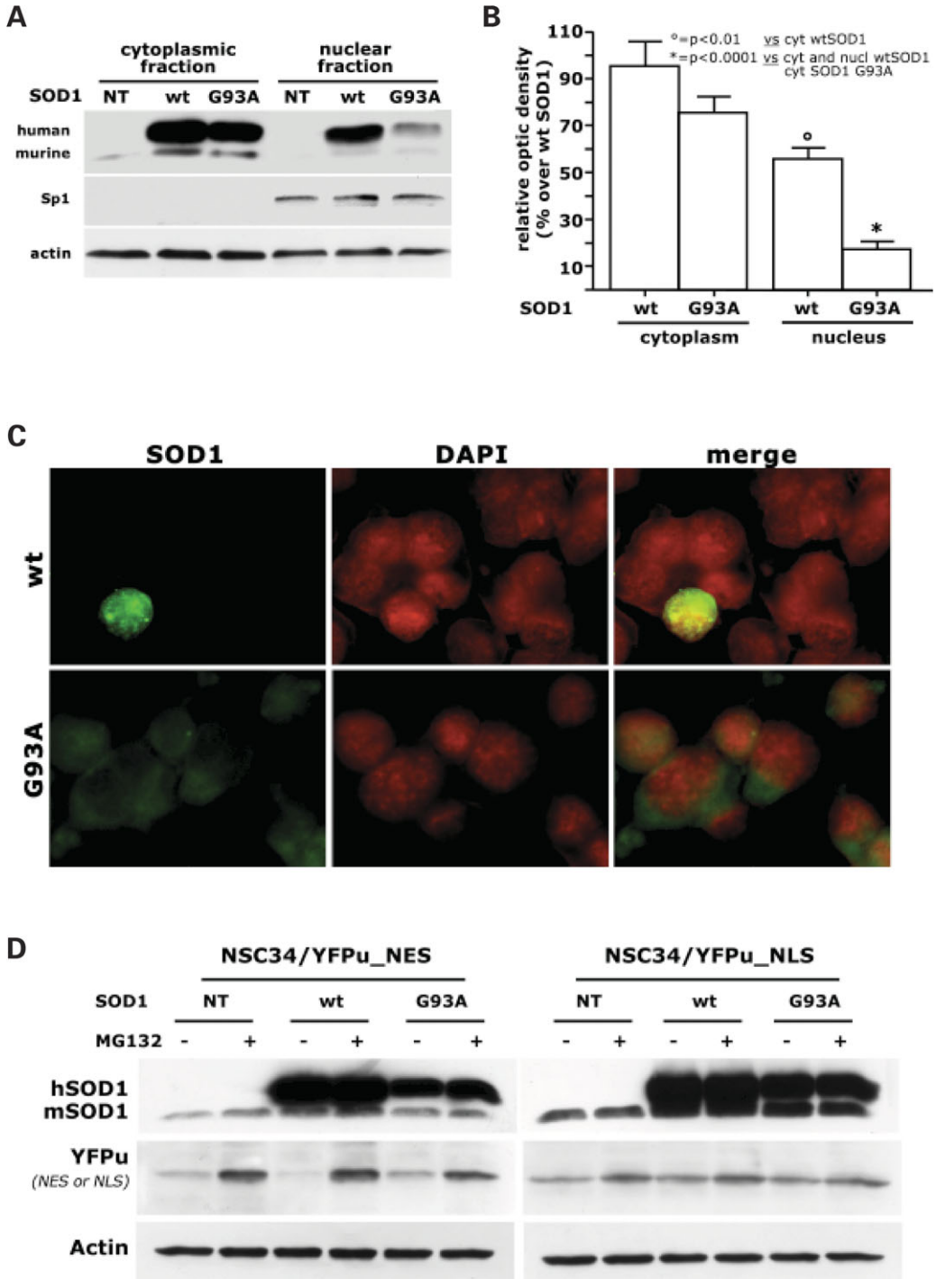

Figure 4. Mutant G93A-SOD1 and nuclear environment. (**A**) Western blot analysis performed on cytoplasmic and nuclear fractions (obtained using NE-PER, see Materials and Methods) obtained from NSC34 transfected with wt or mutant G93A-SOD1. Immunoreactivity for endogenous SOD1 was detected, using a polyclonal anti-SOD1 antibody, in all samples of the two fractions (also in untransfected samples). The nuclear marker Sp1 was used to compare nuclear preparations. Equal protein loading was assayed by evaluating total actin using a polyclonal anti-actin antibody (lower inset, see Materials and Methods) as a control. (**B**) Optic density analysis of the immuno-reactive SOD1 bands identified in western blots from nine independent experiments (the results are the means ± SD). (**C**) Fluorescence microscopy on nucleus obtained from NSC34 cells transfected with wtSOD1 or G93A-SOD1 stained using the anti-SOD1 antibody (green). The nuclei were obtained using a milder purification procedure (see Materials and Methods) to preserve part of the cytoplasmic regions in order to identify SOD1-positive cells. DAPI was utilized to stain the nuclei (red). (**D**) Western blot assays performed on cell lysates of NSC34 co-transfected with wt or mutant G93A-SOD1 and two reporters for cytoplasmic and nuclear proteasome activity: YFPu_NES (expressing a YFPu protein fused with a peptide containing an NES (LALKLAGLDI) (42) from the cAMP-dependent protein kinase inhibitor), left inset, or YFPu_NLS (expressing a YFPu protein fused with a peptide containing an NLS from SV40 large T antigen (PKKKRKV) (43), right inset, in the presence or in the absence of the proteasome inhibitor MG132. Endogenous SOD1 immunoreactivity was detected in all samples, whereas human SOD1 was detected only in transfected samples. Equal protein loading was assayed by evaluating total actin using a polyclonal anti-actin antibody (lower inset, see Materials and Methods) as a control.

detectable in cells expressing the G93A-SOD1. In contrast, no proteasome dysfunctions were observed in the nuclear compartment of NSC34/YFPu_NLS expressing either wt or G93A-SOD1 (Fig. 4D, right blot), thus suggesting that nuclear proteasome activity is not affected by the nuclear G93A-SOD1, even if the mutant SOD1 can form nuclear aggregates. The treatment with the proteasome inhibitor MG132, which increases the intracellular levels of insoluble G93A-SOD1 (see above), did not modify the number of nuclear aggregates found in fluorescence microscopy. As nuclear proteasome activity remains intact and able to remove the misfolded proteins, we have evaluated the possibility that G93A-SOD1 is excluded because more rapidly degraded in the nucleus than the wtSOD1. Time course analyses of wt and G93A-SOD1 nuclear levels, performed after treatment with MG132, have indicated that the levels of both wtSOD1 and G93A-SOD1 increased in the nucleus with time (6, 24, 30 and 48 h after MG132 exposure, data not shown). Unfortunately, the kinetics of SOD1 nuclear levels were influenced by the fact that also the cytoplasmic levels of wt and mutant SOD1s were found to be markedly increased after MG132 treatment. Therefore, based on the kinetic data, it is unclear at present whether G93A-SOD1 exclusion from the nuclei is because of its faster degradation or to a decreased diffusion into the nuclear compartment, and the contribution of these two mechanisms in the G93A-SOD1 nuclear exclusion, cannot be proven until a nuclear-specific proteasome inhibitor becomes available.

Mutant human SOD1 and nuclear damage in NSC34 cells

The results presented so far indicate that SOD1 may remove free radical species not only in the cytoplasm, where it is mainly located, but also in the nucleus. In this latter compartment, wtSOD1 may serve to protect from protein oxidation and/or DNA mutations caused by oxidative stress. We thus investigated whether the generation of free radical species may increase nuclear damage in NSC34 cells expressing G93A-SOD1. To this purpose, we have assayed the DNA integrity in our cellular model of fALS using the Comet assay on cells subjected or not to an oxidative insult. Fig. 5A–D shows an example of Comets with different degrees of damage in the NSC34 cells. The percentage of DNA damage detected following the oxidative treatments is shown in Fig. 5E. Untreated NSC34 cells (Fig. 5A) had a very low percentage of DNA in tail (NSC34 $= 5.1 \pm 0.8$, MUT $= 4.9 \pm 1.1$, WT $= 5.1 \pm 1.1$), thus demonstrating a negligible effect of the experimental procedure on DNA damage. Conversely, the insult with H_2O_2 caused a significant increase of DNA damage in motoneurons (Fig. 5E). The treatment with 10 μM of H_2O_2 was already able to determine approximately 30% DNA damage. The highest level of DNA damage was already obtained using 50 μM of H_2O_2 because similar values (approximately 60% DNA damage) were detected also at H_2O_2 concentrations as high as 100 and 500 μM. Interestingly, the overexpression of either wtSOD1 or G93A-SOD1s protected the nucleus from the free radical damage and significantly reduced the percentage of DNA in tail (particularly at low doses of H_2O_2), suggesting that the exogenous supplement of this enzyme may still increase the antioxidant defense system against free radical species. However, at the highest doses of H_2O_2 tested, only wtSOD1 significantly counteracted the damage to DNA, whereas the protective effect of the G93A-SOD1 was lost. These data demonstrate that during oxidative stress, G93A-SOD1 is less efficient than wtSOD1 in protecting against nuclear damage.

DISCUSSION

The data here presented indicate that, in the nucleus of both motoneurons of transgenic mice and in immortalized motoneurons expressing either human wtSOD1 or mutant SOD1, the levels of mutant SOD1 are reduced compared with those of wtSOD1. This may be because of the formation of insoluble high MW species of mutant SOD1 that prevent the diffusion of the protein across the nuclear membrane, whereas this diffusion is possible for wtSOD1. An alternative possibility is that mutant SOD1 nuclear deprivation might be because of its faster turnover in this compartment when compared with wtSOD1.

Reduced levels of G93A-SOD1 may reflect a decrease of its enzymatic activity and, thus, a decreased removal of free radical species inside the nucleus. The obvious consequence of the loss of this protective function of SOD1 in the nucleus is that genomic DNA may be more easily altered by the attack of reactive species; this, in turn, may induce DNA damage, and consequently, alterations in the protein expression profile in motoneurons.

Our data are in contrast to those of Wate *et al*. (30), who found no correlation between SOD1 expression and nuclear DNA damage in Tg G93A-SOD1 mice using the Comet assay. Methodological differences may explain this discrepancy as we used immortalized motoneuronal cells instead of fibroblasts derived from Tg G93A-SOD1 mice kidney. It is reasonable to assume that the mechanism we describe is relevant only in motoneurons because of their selective vulnerability in ALS. Moreover, to induce the nuclear DNA insults we used H_2O_2, which is likely to be more directly involved than γ-ray irradiation in the induction of an oxidative damage in ALS.

Interestingly, knockout mice lacking SOD1 (koSOD1) have been shown to develop normally and their spinal cord apparently had no signs of pathology (31), suggesting that SOD1 is not necessary for normal motoneurons development and functions. However, SOD1 seems to be required under physiological stressful conditions. In fact, after facial axotomy, the koSOD1 mice displayed more extensive loss of facial motoneurons than either heterozygous or wt mice (31). It must also be noted that the same koSOD1 mice developed, at 6 months of age, subtle motor symptoms (6), which were distinct from those typical of human ALS seen in Tg G93A-SOD1 mice, and exhibited impairment of axonal sprouting and reinnervation of denervated muscle fibers. It has also been shown that, compared with wt control mice, heterozygous koSOD1 mice showed 30% mortality after ischemia, neurological deficits were exacerbated and accompanied by increased apoptotic neuronal cell death; this

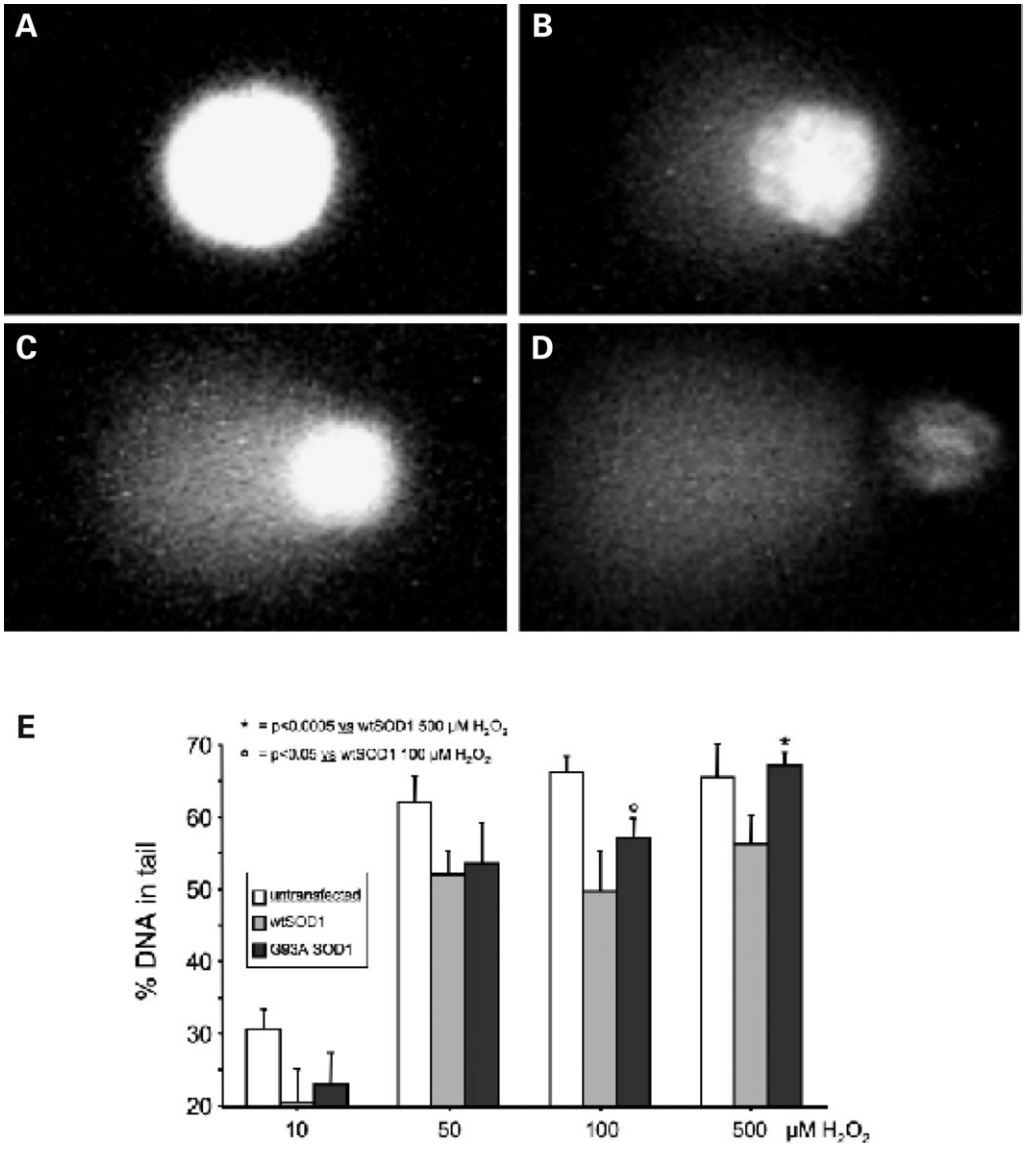

Figure 5. Mutant SOD1 and nuclear damage. Analysis of nuclear damage, after induction of oxidative stress, through evaluation of fragmented DNA with Comet assay (see Materials and Methods). (**A**–**D**) Example of Comets, with different degree of damage, respectively: (A) no damaged, (B) low damaged, (C) high damaged and (D) very high damaged DNA, performed on untransfected NSC34 cells, treated with H_2O_2. (**E**) Evaluation of DNA damage, measured as % DNA in tail (i.e. fluorescence intensity in tail/total fluorescence intensity), in untransfected cells or cells expressing either wt or G93A-SOD1 treated with different concentrations of H_2O_2.

suggests that the loss of protection from oxygen free radicals, especially superoxide anions, may contribute to apoptotic neuronal cell death even after focal cerebral ischemia and reperfusion (32).

These data, therefore, suggest that a reduced SOD1 activity, although not sufficient to induce neurodegeneration, is able to affect motoneurons (6). In line with this, cells derived from SOD1-deficient mice are highly sensitive to oxygen toxicity (33). Thus, despite the fALS phenotype in animals is generated only by the expression of the mutant human SOD1 (34), a reduction of SOD1 efficacy in removing free radical species may contribute to the onset and progression of the disease. Indeed, it has recently been shown that, in Tg G93A-SOD1 mice, but not in control tg wtSOD1 mice, elevated nitrated and oxidized proteins are present in neurons of the motor cortex, of the cerebellar cortex and of nucleus of hypoglossal nerves (35); this correlates *in vivo* SOD1 mutation to nitration and oxidation of neurons located in the movement regions. Interestingly, in the same animals, neurons in the motor cortex are significantly more sensitive to nitration and oxidation than those in the sensory cortex, suggesting that a SOD1 loss of function may enhance susceptibility of the motor cortex to nitration and oxidation of proteins (35). In our experiments, mutant human SOD1 did not alter the survival rate of immortalized motoneuron cell lines, even in the presence of toxic doses of hydrogen peroxide. The tests were performed using the MTT assay on NSC34 cells expressing full-length wt or mutant SOD1s as well as

the same proteins targeted to the nucleus or to the cytoplasm (not shown). Our results are in line with those reported by Takeuchi *et al*. (36) in Neuro2a cells, showing that only mutant SOD1 targeted to mitochondria, and not the one targeted to the nucleus, impairs neuronal survival.

The combination of the gain-of-neurotoxic-function with the loss-of-nuclear-protection exerted by mutant SOD1 may, therefore, be necessary to generate the fALS phenotype, and it is reasonable to postulate that the two mechanisms may cooperate mutually. However, Bruijn *et al*. (37) have shown that the genetic ablation of endogenous SOD1 (as well as the overexpression of human wtSOD1) has no effect on mutant SOD1-mediated disease in mice expressing a mutant SOD1 lacking its enzymatic activity (G85R-SOD1). This discrepancy with our results may be due to the fact that DNA damage derived from the altered solubility of mutant SOD1 is not the primary cause, but a contributing factor for disease progression. In fact, it must be noted that although these animals had a mean survival age of approximately 1 year, SOD1-fALS patients are likely exposed to nuclear de-protection from free radical species for decades prior to symptoms appearance. This very large time window of exposure to ROS in the nuclei may allow accumulation of DNA mutations also in genes potentially relevant for neuronal functions, making motoneurons more sensitive to mutant SOD1 toxicity. More recently, Deng *et al*. (29), using double-transgenic mice overexpressing both wt and mutant human SOD1, demonstrated that human wtSOD1 is able to exacerbate the ALS-like disease progression and to form aggregates, thus suggesting that the conversion into an insoluble status, that segregates the active enzyme, may be sufficient to induce the pathological conditions. Moreover, the authors also showed that human wtSOD1 is able to convert a mutant transgenic mouse line (A4V-SOD1) from an unaffected phenotype to an ALS-like pathological phenotype (29). This may explain why in our study the DNA damage cannot be prevented by the endogenous mouse SOD1 in the presence of the mutant exogenous G93A-SOD1. Interestingly, in our experiments the expression of mutant SOD1 correlates with a reduction of the endogenous mouse SOD1, and this may also explain the reduced protection from the oxidative damage at the DNA level. Several data are indeed accumulating showing that the levels of oxidative damage to DNA are increased in sALS patients (10,11) and in an animal model of ALS (12). Moreover, the existence of nuclear aggregates in motoneurons of an ALS patient has also been recently reported (9). As in motoneurons of fALS patients mutant SOD1 is expressed from the beginning of life, whereas other mutations activated by DNA damage likely follow a progressive accumulation over the years, the mechanisms here proposed may help to understand the lack of correlation between age of onset and disease progression normally found in fALS. In this regard, it is also interesting to mention that alterations in nuclear cell cycle regulators detected in motoneuron of ALS patients have been suggested to participate in molecular mechanisms regulating motoneuron death (38).

On the basis of our results, showing that G93A-SOD1 is excluded from the nucleus, the effect we have observed could be at least in part ascribed to the increased nuclear concentration of free radical species due to a lower clearance in the nucleus. It remains to be determined whether the altered intracellular distribution of G93A-SOD1 may be counteracted by compounds that are able to reduce SOD1 aggregation (such as chaperones), and, if so, whether these compounds may also reduce DNA damage in Comet assays. Interestingly, although the activity of 'normally folded' mutant SOD1s is not generally altered in most mutations (see 1 for a review), it has been shown that (39) in erythrocyte lysates of SOD1-linked fALS patients (including six different SOD1 mutations), the concentration and specific activity of SOD1 are decreased relative to controls (51 and 46%, respectively), whereas the apparent turnover number of the enzyme was not altered, suggesting that mutant SOD1 is unstable in these cells. No correlation between enzyme concentration, or specific activity, and disease severity was found, and thus the indirect effect of mutant SOD1 on DNA quality may provide a novel explanation for this apparent discrepancy.

Finally, Kato *et al*. (40) have demonstrated that SOD1 neuronal inclusions in the spinal cords of fALS patients and (H46R or G93A) SOD1 tg mice contain peroxiredoxin-2 (Prx2, thioredoxin peroxidase) and glutathione peroxidase-1 (GPx1), two enzymes involved in the conversion of ROSs to oxygen (O2) which act in conjunction with SOD1. Therefore, SOD1 aggregation may lead to alteration of the redox system itself, thus amplifying the mutant SOD1-mediated toxicity (32).

In any case, the data obtained strongly suggest that the nucleus is a previously unrecognized target of G93A-SOD1 neurotoxicity in fALS and that the point mutations in SOD1 may indirectly determine a regional (subcellular?) 'loss of function' of the aberrant enzyme.

MATERIALS AND METHODS

Materials

All chemicals have been obtained from Sigma (St Louis, MI, USA).

Plasmids

The plasmids pcDNA3-wtSOD1 and pcDNA3-G93A-SOD1, expressing the hSOD1 wt or containing the G93A mutation, routinely used in our laboratory have been previously published (41).

The plasmids pECFP-wtSOD1 and pECFP-G93A-SOD1, expressing wt or mutant human SOD1 tagged with *Cyan Fluorescent Protein* (CFP), a cyan fluorescent variant of green fluorescent protein (GFP) derived from *Aequorea victoria*, have been obtained by inserting the *Bam*HI/*Apa*I cDNA fragments (595 bp) coding for the wt or mutant SOD1s (excised from pcDNA3-wtSOD1 or from pcDNA3-G93A-SOD1, respectively) 'in frame' with the CFP cDNA into the *Bgl*II/*Apa*I sites of pECFP-C1 (Clontech Lab., Palo Alto, CA, USA). The resulting plasmids have been sequenced to exclude any potential mutation in the coding sequence of the chimeric proteins.

The plasmid YFPu derives from the GFPu (kindly provided by Ron Kopito, Stanford University, Stanford, CA, USA) (27); in the new plasmid, the cDNA coding for the CL1 degron (see

below) was inserted into the pEYFP-C1 (Clontech Lab., Palo Alto, CA, USA) backbone using the *Xho*I/*Bam*HI sites (22). The plasmid YFPu-NES expresses a YFPu protein fused with a peptide containing an NES (LALKLAGLDI) (42) from the cAMP-dependent protein kinase inhibitor, to assay ubiquitin-proteasome pathway function in the cytoplasm (22); the plasmid YFPu-NLS expresses a YFPu protein fused with a peptide containing an NLS from SV40 large T antigen (PKKKRKV) (43) to assay ubiquitin-proteasome pathway function in the nuclei (22).

The plasmids YFP-NLS-wtSOD1, YFP-NES-wtSOD1, YFP-NLS-G93A-SOD1 and YFP-NES-G93A-SOD1, derive from the pcDNA3-wtSOD1 or pcDNA3-G93A-SOD1 plasmids and YFPu-NLS or YFPu-NES. To prepare these vectors, the *Kpn*I/*Apa*I cDNA fragment coding for wt or mutant SOD1s (excised from pcDNA3-wtSOD1 or from pcDNA3-SOD1-G93A, respectively) has been inserted 'in frame' with the cDNA sequences coding for the YFPu-NLS or YFPu-NES into the corresponding *Kpn*I/*Apa*I sites of the plasmids described above; using this strategy, the cDNA sequence coding for CL1 degron was lost after the excision of the *KpnI/ ApaI* digested fragment and the resulting proteins expressed contain the YFP/(NLS or NES)/SOD1 (wt or mutant) chimera.

Cell Cultures

The immortalized motoneuron cell line, NSC34 (kindly provided by Dr N.R. Cashman, McGill University, Montreal, Canada) (17) has been routinely maintained as previously described (20,21). Transient transfections were performed using Lipofectamine Plus as previously described (21). Transient transfections for immunofluorescence analysis were performed using 1 μg of plasmid coding for wt and G93A-SOD1, 4 μl of transferrin solution and 2 μl of Lipofectamine for each sample.

Transient transfections for immunofluorescence and fluorescence microscopy analyses were performed on NSC34 plated in 12-well multiwell plates, with glass coverslips, plated at 70 000 cells/ml density and transfected using 1 μg pECFP-SOD1s plasmids, YFP-NLS-SOD1s or YFP-NES-SOD1s plasmids were all performed using of plasmid 6 μl of transferrin solution and 4 μl of Lipofectamine for each sample.

Samples for western blot analysis of proteasome functions were obtained by co-transfecting 1.9 μg of wt or G93A-SOD1s plasmid and 0.1 μg of YFPu (also NES-YFPu, or NLS-YFPu) plasmid, 6 μl of transferrin solution and 4 μl of Lipofectamine for each sample.

Transient transfections for western blot assays were performed using 2 μg of wt or G93A-SOD1 plasmid, 6 μl of transferrin solution and 4 μl of Lipofectamine for each sample, whereas transient transfections for COMET assay were performed using 4 μg of wt or G93A-SOD1 plasmids, 6 μl of transferrin solution and 4 μl of Lipofectamine for each sample.

Animals

Mice were maintained at a temperature of 21 ± 1°C with a relative humidity 55 ± 10% and 12 h of light. Food (standard pellets) and water were supplied *ad libitum*. Transgenic mice originally obtained from Jackson Laboratories and expressing a high copy number of mutant human SOD1 with a Gly-93-Ala substitution (G93A-SOD1) (5) or wt human SOD1 (wtSOD1) mice were bred and maintained on a C57BL/6 mice strain at the Consorzio Mario Negri Sud, S. Maria Imbaro (CH), Italy. Transgenic mice were identified by polymerase chain reaction (4).

Procedures involving animals and their care were conducted in conformity with the institutional guidelines that are in compliance with national (D.L. No. 116, G.U. suppl. 40, February 18, 1992, Circolare No. 8, G.U., 14 luglio 1994) and international laws and policies (EEC Council Directive 86/609, OJ L 358, 1 December 12, 1987; NIH Guide for the Care and use of Laboratory Animals, U.S. National Research Council, 1996). All efforts were made to minimize the number of animals used and their suffering.

We used female G93A-SOD1 mice at the following weeks of age: 6 (early presymptomatic), 15 (early symptomatic) and 19 (late stage of the progression of motor dysfunction). Females expressing human wtSOD1 at 15 and 19 weeks of age or non-transgenic age-matched littermates were used as controls. Three animals per group and per age were analyzed.

Immunocytochemistry

Mice were anesthetized with Equithesin (1% phenobarbitol/4% v/v chloral hydrate, 30 μL/10 g, i.p.) and transcardially perfused with 20 mL saline followed by 50 mL of sodium-phosphate-buffered 4% paraformaldehyde solution. Spinal cords were removed, post-fixed in fixative for 2 h and then either embedded in paraffin or sliced with a vibratome or frozen. Light microscopic immunocytochemical analyses were done on lumbar spinal cord sections (10 μm thick paraffin sections collected on slides; 40 μm thick floating vibratome sections and 20 μm thick floating cryosections).

The following primary antibodies were used: (1) monoclonal anti-human SOD1 (MO62-3, clone 1G2, directed against the full-length human SOD1 protein; MBL, Japan; dilution 1:3000); (2) polyclonal anti-SOD1 (SOD-100, Stress-Gen, dilution 1:200).

For the immunoperoxidase procedure, tissue sections were treated with 1% hydrogen peroxide in PBS to inhibit endogenous peroxidases, blocked in 1% BSA in PBS containing 0.2% Triton X-100 for 30 min and then incubated overnight with the primary antibodies diluted in PBS containing 0.1% BSA. Immune reactions were revealed by 75 min incubation in the appropriate secondary biotinylated antiserum (goat anti-rabbit for the polyclonal and horse anti-mouse for the monoclonal, both from Vector Laboratories and diluted 1:200), followed by 75 min incubation in the Avidin-Biotin-peroxidase Complex (ABC, Vector) and using diaminobenzidine as chromogen. For immunofluorescence, the following highly preabsorbed secondary antibodies were used, all diluted 1:200 in PBS–0.1% BSA:goat anti-rabbit IgG conjugated to Alexa 488 and goat anti-mouse IgG conjugated to Alexa 564 (Molecular Probes). Control sections processed with omission of the primary antiserum and developed under the same conditions gave no immunostaining.

Nissl substance was stained with NeuroTrace™ 640/660 deep red-fluorescent Nissl stain (Molecular Probes) according to the manufacturer's instructions. Sections were examined under a TCS NT confocal laser scanning microscope (Leica Lasertecknik GmbH, Heidelberg, Germany) equipped with a 75-mW Kripton/Argon mixed gas laser. Fluorochromes were excited at 488 and 568 nm, visualized, respectively, with a 530/30 nm and a 600 nm band-pass filters, imaged separately and merged with Leica Power Scan software.

Immunofluorescence and microscopy

The cells were plated at 70 000 cells/mL in 12-well multiwell plates, containing 18-mm glass coverslips in DMEM plus 5% FBS and subsequently transfected with wt or G93A-SOD1. Cells were allowed to grow for 48 h and then fixed using a 1:1 solution of 4% saccharose and 4% paraformaldeyde in 0.2 N PB (25 min at 37°C under weak agitation), and then in ice-cold methanol (10 min at room temperature). Fixed cells were then washed with low salt buffer (LS, 4% PB 0.2 M, 4% NaCl 4 M, in H_2O), 3 times × 5 min at room temperature, and high salt buffer (HS, 8% PB 0.2 M, 12% NaCl 4 M, in H_2O), 3 times × 5 min at room temperature; then permeabilized with 2% Triton X-100 in PBS 10 min at room temperature. Samples were then treated with a blocking solution containing 5% non-fat dry milk in Tween-TBS (TBS-T, 20 mM Tris–HCl, pH 7.5, 0.5 M NaCl, 0.05% Tween-20) for 1 h to block aspecific protein binding sites and were then incubated, o/n at 4°C, with the primary antibody (rabbit polyclonal anti-SOD1, SOD-100 from Stressgen, Victoria, BC, Canada; dilution 1:200 in milk) to detect wt and G93A-SOD1. Cells were then washed with buffer HS, 3 times × 10 min, and incubated with secondary antibody (Alexa FITC anti rabbit, Molecular Probes, Eugene, USA; dilution 1:1000 in milk), 1 h RT. Samples were finally washed with buffer LS (3 times × 5 min) and HS (3 times × 5 min).

To routinely analyze transfection efficiency in living immortalized motoneuronal cells, and to measure the number and size of aggregates in the cell cytoplasm and in the nuclei, an Axiovert 200 microscope (Zeiss Instr., Oberkochen, Germany) equipped with FITC filters for fluorescence analysis was used throughout the study. Fluorescence images were captured by a Photometric CoolSnap CCD camera (Ropper Scientific, Trenton, NJ, USA). Images were processed using Metamorph software (Universal Imaging, Downingtown, PA), whereas images deconvolution was performed using the AutoDeblur program (AutoQuant Imaging, Inc., Watervliet, NY, USA). Localization of SOD1 nuclear aggregates was characterized using the TCS NT confocal laser scanning microscope (Leica Lasertecknik GmbH, Heidelberg, Germany).

ICC was performed using the anti-SOD1 antibody as described above. Immortalized motoneurons were then analyzed in fluorescence microscopy to count the number of aggregates formed per cells. The number of G93A-SOD1 transfected NSC34 cells bearing aggregates was estimated using a PL 10X/20 eyepiece with graticules (100 × 10 mM in a 100-grid divisions). The percentage of the cells with aggregates was obtained by dividing the number of the cells with aggregates by the total number of the transfected cells. The percentage of the cells with cytoplasmic aggregates was obtained by dividing the number of the cells with cytoplasmic aggregates by the total number of the transfected cells. The percentage of the cells with nuclear aggregates was obtained by dividing the number of the cells with nuclear aggregates by the total number of the transfected cells. The percentage of the cells with both cytoplasmic and nuclear aggregates was obtained by dividing the number of the cells with both cytoplasmic and nuclear aggregates by the total number of the transfected cells. Three different fields were analyzed for each slide; each point was done in triplicate.

Transfected cells were scored by their staining pattern as having nuclear or cytoplasmic aggregates. Measure of nuclear and cytoplasmic integrated intensity was obtained by analyzing all images of cells immunolabeled for human SOD1 staining (both wt or mutant) using threshold measure tools in Metamorph software; three different fields were analyzed for each sample.

To analyze hSOD1 immunostaining in the nuclear compartment, we used a mild procedure instead of the NE-PER protocol (see below); briefly, the nuclei from NSC34 transfected with wt or mutant SOD1 have been purified by harvesting the cells in medium, followed by centrifugation at 100*g* for 5 min (4°C); the pellets were washed with PBS, and the cells were then resuspended in 70% EtOH in 0.9% NaCl, centrifuged at 400*g* for 5 min (4°C). The pellets were resuspended in ice-cold PBS, centrifuged at 400*g* for 5 min (4°C). The pellets containing nuclei were resuspended in 50 μl of ice-cold 0.01 M PBS; spots containing nuclei were spotted on poly-prep slides coated with poly-L-lysine (Sigma), and dried at RT. Slides were washed in H_2O and twice in PBS at RT, treated 5 min at RT with 0.1% Triton X-100, then washed with PBS. Immunofluorescence for hSOD1 on extracted nuclei was then performed as described above.

Western blot analysis and filter retardation assay

The cells transfected as above described were harvested and centrifuged 5 min at 100*g*; the pellets of cells were resuspended in PBS (added of the protease inhibitors cocktail, Sigma) and homogenized using slight sonication. Total proteins were determined with the bicinchoninic acid method (BCA assay, Pierce, Rockford, IL, USA). Western immunoblot analysis was performed by SDS–polyacrylamide gel electrophoresis (PAGE) resolution of the samples obtained from NSC34-transfected cells after 48 h of transfection. Samples containing 30 μg of total proteins were heated to 100°C for 5 min in sample buffer (0.6 g/100 mL Tris, 2 g/100 mL SDS, 10% glycerol, 1% β-mercaptoethanol, pH 6.8) and loaded onto 12% SDS–PAGE gel, after which they were electrotransferred to nitrocellulose membranes (*Trans*-blot, Bio-Rad Laboratories, Hercules, CA, USA) using a liquid transfer apparatus (Bio-Rad). Nitrocellulose membranes were treated with a blocking solution containing 5% non-fat dry milk in TBS-T for 1 h to block aspecific protein binding sites and were then incubated with the primary antibodies: (a) mouse monoclonal anti-GFP (clone C163; Zymed, San Francisco, CA, USA; dilution 1:1000) to detect YFPu, YFPu-NES, YFPu-NLS; (b) rabbit polyclonal anti-Cu/Zn superoxide dismutase SOD1 (SOD-100; Stressgen, Victoria, BC Canada; dilution 1:1000) to detect the wt and G93A-SOD1

proteins or (c) goat polyclonal anti-Actin (Actin I-19; Santa Cruz dilution 1:1000) to detect total actin; (d) rabbit polyclonal antibody against Sp1 (clone PEP2, Santa Cruz dilution 1:500). Immunoreactivity was detected using the following secondary peroxidase-conjugated antibodies: goat anti-rabbit (sc-2004, Lot: C3006, Santa Cruz) was used to identify the anti-SOD1 and Sp1 antibodies; goat anti-mouse (sc-2005, Lot: A0405, Santa Cruz) was used to identify the anti-GFP antibody; donkey anti-goat (sc-2020, Lot: J2303, Santa Cruz) was used to identify the anti-Actin antibody. The immunoreactive regions were then visualized using the enhanced chemiluminescence detection kit reagents (ECL, Amersham, Little Chalfont, Buckinghamshire, UK). The same membranes were subsequently processed with antibodies (a)–(d) to detect the levels of YFP-based proteins, SOD1 and actin protein in the same samples loaded on the gel. To this purpose, primary and secondary antibodies were removed from the membrane by incubation for 15 min at 37°C in Restore Western Blotting stripping buffer (Pierce) and then washing twice with TBS-T, and then the membranes were processed as described above.

Extraction of nuclear and cytoplasmic proteins for western blotting was performed using NE-PER Nuclear and Cytoplasmic Extraction Reagents (Pierce) according to the manufacturer's protocol. Total proteins were determined with the bicinchoninic acid method, and Western immunoblot analysis was done as previously described, loading 40 μg of cytoplasmic proteins and a corresponding value of nuclear extracts (estimated by the dilution ratio 1:2 maintained between nuclear and cytoplasmic fractions) onto 12% SDS–PAGE gel.

Filtration of proteins through a 0.2 μm cellulose acetate membrane (Schleicher&Schuell Microscience, Dassel, Germany) was performed using a slot-blot apparatus (Bio-Rad). The membranes were treated with 20% methanol, rinsed first in water and then washed in PBS buffer. Samples of protein (0.75 μg) were prepared in a final volume of 50 μl in PBS, loaded and gently vacuumed. Membranes were washed twice with PBS, then rinsed with 20% methanol and finally in water. Slot-blots were probed as described for western blots.

Optical intensity of samples assayed with both filter retardation assay and western blot was detected and analyzed using NIH ImageJ software.

Determination of DNA damage by Comet assay

Comet assay allows the evaluation of single-strand breaks in DNA by determining the quantity of DNA migrated from the nucleus towards the anode after electrophoresis (damaged DNA exhibits a comet shape). It was applied as previously described (44) and used to evaluate DNA damage in NSC34, non-transfected and transfected with wt or G93A-SOD1, treated with different doses of H_2O_2 (10–500 μmol/L).

For the Comet analysis, 150 μl of cell suspensions (about 10 000 cells in DMEM) were spun 5 min at 100*g* at 4°C and the pellet resuspended in 50 μL serum-free DMEM. Low-melting-point agarose (LMP 1.5%, 120 μL) was mixed and about 50 μL of the final cell suspension was pipetted onto fully frosted microscope slides (Richardson Supply Co., London, UK) previously added with an agarose layer (1%, 100 μL). A coverslip was added and solidification was obtained at 4°C in the dark. A second layer of LMP (100 μL) was added and left to solidify as previously described. Coverslips were then removed for the oxidative treatment and slides were put in cold PBS containing the different concentrations of H_2O_2, whereas control slides were maintained in PBS for the same time (5 min). The experiment was performed in triplicate.

After the oxidative treatment, cells on slides were put in a cold lysing solution (2.5 M NaCl, 100 mM Na_2EDTA, 10 mM Tris, pH 10 added with 1% Triton, 1% DMSO) for 1 h at 4°C. Then, slides were put in a horizontal electrophoresis tank (Scotlab, Coatbridge, UK), filled with fresh electrophoresis solution (1 mM Na_2EDTA, 300 mM NaOH) and left for 40 min before electrophoresis (300 mA, 25 V, 20 min). After neutralization (0.4 M Tris, pH 7.5, 15 min) cells on slides were stained with ethidium bromide (2 μg/mL).

Individual cells or 'Comets' were analyzed at 400× magnification using an epifluorescence microscope (BX 60 OLYMPUS) equipped with an excitation filter BP520-550, dichroic beam-splitter DM565 and BA580-IF barrier filter (OLYMPUS, Olympus Italia s.r.l., Milan, Italy). The light source was a 100 W Hg lamp (OLYMPUS). The microscope was attached to a high-sensitivity CCD video camera and to a computer provided with an image analysis system (Comet Programme exploited on Image Pro-Plus, Immagini e Computer, Bareggio, Milan, Italy) and set to calculate the DNA damage (% DNA in tail) in treated and control cells.

Statistical analysis

Statistical analysis has been performed using one-tailed Student's *t*-test by utilizing the PRISM software (version 4.0b, GraphPad Software, Inc., San Diego, CA, USA). MANOVA with cell type (untransfected, wtSOD1 and G93A-SOD1) and oxidative treatment (10, 50, 100, 500 μmol/L H_2O_2) as factors was used for the analysis of data on DNA damage.

ACKNOWLEDGEMENTS

The financial support of Telethon-Italy (Grants no. #1283, GP0222Y01 and GGP06063), the Italian Ministry of University and Research (MIUR-FIRB #RBAU01NXFP), MIUR-Cofin (2003054414_003 and 2005057598_002), the Italian Ministry of Health convenzione No. 93, FONDAZIONE CARIPLO and the University of Milan (FIRST 05 and 06) is gratefully acknowledged. Confocal microscopy was carried out at the Centro Interdipartimentale di Microscopia Avanzata (CIMA) of the University of Milan. The authors thank Dr N.R. Cashman (University of Toronto, Ontario, Canada) for having provided the NSC34 cells, and Prof. Ron K. Kopito (Stanford University, Stanford, CA, USA) for having provided the GFPu vector.

Conflict of Interest statement. None declared.

REFERENCES

1. Bendotti, C. and Carri, M.T. (2004) Lessons from models of SOD1-linked familial ALS. *Trends Mol. Med.*, **10**, 393–400.
2. Boillée, S., Vande Velde, C. and Cleveland, D.W. (2006) ALS: a disease of motor neurons and their nonneuronal neighbors. *Neuron*, **52**, 39–59.
3. Pasinelli, P. and Brown, R.H. (2006) Molecular biology of amyotrophic lateral sclerosis: insights from genetics. *Nat. Rev. Neurosci.*, **7**, 710–723.
4. Rosen, D.R., Siddique, T., Patterson, D., Figlewicz, D.A., Sapp, P., Hentati, A., Donaldson, D., Goto, J., O'Regan, J.P., Deng, H.X. *et al.* (1993) Mutations in Cu/Zn superoxide dismutase gene are associated with familial amyotrophic lateral sclerosis. *Nature*, **362**, 59–62.
5. Gurney, M.E., Pu, H., Chiu, A.Y., Dal Canto, M.C., Polchow, C.Y., Alexander, D.D., Caliendo, J., Hentati, A., Kwon, Y.W., Deng, H.X. *et al.* (1994) Motor neuron degeneration in mice that express a human Cu, Zn superoxide dismutase mutation. *Science*, **264**, 1772–1775.
6. Shefner, J.M., Reaume, A.G., Flood, D.G., Scott, R.W., Kowall, N.W., Ferrante, R.J., Siwek, D.F., Upton-Rice, M. and Brown, R.H., Jr (1999) Mice lacking cytosolic copper/zinc superoxide dismutase display a distinctive motor axonopathy. *Neurology*, **53**, 1239–1246.
7. Khare, S.D., Wilcox, K.C., Gong, P. and Dokholyan, N.V. (2005) Sequence and structural determinants of Cu,Zn superoxide dismutase aggregation. *Proteins*, **3**, 617–632.
8. Valentine, J.S., Doucette, P.A. and Zittin Potter, S. (2005) Copper—zinc superoxide dismutase and amyotrophic lateral sclerosis. *Annu. Rev. Biochem.*, **74**, 563–593.
9. Seilhean, D., Takahashi, J., El Hachimi, K.H., Fujigasaki, H., Lebre, A.S., Biancalana, V., Durr, A., Salachas, F., Hogenhuis, J., de The, H. *et al.* (2004) Amyotrophic lateral sclerosis with neuronal intranuclear protein inclusions. *Acta Neuropathol. (Berl)*, **108**, 81–87.
10. Fitzmaurice, P.S., Shaw, I.C., Kleiner, H.E., Miller, R.T., Monks, T.J., Lau, S.S., Mitchell, J.D. and Lynch, P.G. (1996) Evidence for DNA damage in amyotrophic lateral sclerosis. *Muscle Nerve*, **19**, 797–798.
11. Bogdanov, M., Brown, R.H., Matson, W., Smart, R., Hayden, D., O'Donnell, H., Flint Beal, M. and Cudkowicz, M. (2000) Increased oxidative damage to DNA in ALS patients. *Free Radic. Biol. Med.*, **29**, 652–658.
12. Aguirre, N., Beal, M.F., Matson, W.R. and Bogdanov, M.B. (2005) Increased oxidative damage to DNA in an animal model of amyotrophic lateral sclerosis. *Free Radic. Res.*, **39**, 383–388.
13. Barber, S.C., Mead, R.J. and Shaw, P.J. (2006) Oxidative stress in ALS: a mechanism of neurodegeneration and a therapeutic target. *Biochim. Biophys. Acta*, **1762**, 1051–1067.
14. Bendotti, C., Calvaresi, N., Chiveri, L., Prelle, A., Moggio, M., Braga, M., Silani, V. and De Biasi, S. (2001) Early vacuolization and mitochondrial damage in motor neurons of FALS mice are not associated with apoptosis or with changes in cytochrome oxidase histochemical reactivity. *J. Neurol. Sci.*, **191**, 25–33.
15. Wong, P.C., Pardo, C.A., Borchelt, D.R., Lee, M.K., Copeland, N.G., Jenkins, N.A., Sisodia, S.S., Cleveland, D.W. and Price, D.L. (1995) An adverse property of a familial ALS-linked SOD1 mutation causes motor neuron disease characterized by vacuolar degeneration of mitochondria. *Neuron*, **14**, 1105–1116.
16. Kong, J. and Xu, Z. (1998) Massive mitochondrial degeneration in motor neurons triggers the onset of amyotrophic lateral sclerosis in mice expressing a mutant SOD1. *J. Neurosci.*, **18**, 3241–3250.
17. Cashman, N.R., Durham, H.D., Blusztajn, J.K., Oda, K., Tabira, T., Shaw, I.T., Dahrouge, S. and Antel, J.P. (1992) Neuroblastoma × spinal cord (NSC) hybrid cell lines resemble developing motor neurons. *Dev. Dyn.*, **194**, 209–221.
18. Durham, H.D., Dahrouge, S. and Cashman, N.R. (1992) Evaluation of the spinal cord neuron × neuroblastoma hybrid cell line NSC-34 as a model for neurotoxicity testing. *Neurotoxicology*, **14**, 387–395.
19. Marron, T.U., Guerini, V., Rusmini, P., Sau, D., Brevini, T.A.L., Martini, L. and Poletti, A. (2005) Androgen-induced neurite outgrowth is mediated by neuritin in motor neurones. *J. Neurochem.*, **92**, 10–20.
20. Piccioni, F., Pinton, P., Simeoni, S., Pozzi, P., Fascio, U., Vismara, G., Martini, L., Rizzuto, R. and Poletti, A. (2002) Androgen receptor with elongated polyglutamine tract forms aggregates that alter axonal trafficking and mitochondrial distribution in motor neuronal processes. *FASEB J.*, **160**, 1418–1420.
21. Simeoni, S., Mancini, M.A., Stenoien, D.L., Marcelli, M., Weigel, N.L., Zanisi, M., Martini, L. and Poletti, A. (2000) Motoneuronal cell death is not correlated with aggregate formation of androgen receptors containing an elongated polyglutamine tract. *Hum. Mol. Genet.*, **9**, 133–144.
22. Rusmini, P., Sau, D., Crippa, V., Palazzolo, I., Simonini, F., Onesto, E., Martini, L. and Poletti, A. (2006) Aggregation and proteasome: the case of elongated polyglutamine aggregation in spinal and bulbar muscular atrophy. *Neurobiol. Aging*, **28**, 1099–1111.
23. La Spada, A.R., Wilson, E.M., Lubahn, D.B., Harding, A.E. and Fischbeck, K.H. (1991) Androgen receptor gene mutations in X-linked spinal and bulbar muscular atrophy. *Nature*, **352**, 77–79.
24. Poletti, A. (2004) The polyglutamine tract of androgen receptor: from functions to dysfunctions in motor neurons. *Front. Neuroendocrinol.*, **25**, 1–26.
25. Wanker, E.E., Scherzinger, E., Heiser, V., Sittler, A., Eickhoff, H. and Lehrach, H. (1999) Membrane filter assay for detection of amyloid-like polyglutamine-containing protein aggregates. *Methods Enzymol.*, **309**, 375–386.
26. Koyama, S., Arawaka, S., Chang-Hong, R., Wada, M., Kawanami, T., Kurita, K., Kato, M., Nagai, M., Aoki, M., Itoyama, Y. *et al.* (2006) Alteration of familial ALS-linked mutant SOD1 solubility with disease progression: its modulation by the proteasome and Hsp70. *Biochem. Biophys. Res. Commun.*, **343**, 719–730.
27. Bence, N.F., Sampat, R.M. and Kopito, R.R. (2001) Impairment of the ubiquitin-proteasome system by protein aggregation. *Science*, **292**, 1552–1555.
28. Bennett, E.J., Bence, N.F., Jayakumar, R. and Kopito, R.R. (2005) Global impairment of the ubiquitin-proteasome system by nuclear or cytoplasmic protein aggregates precedes inclusion body formation. *Mol. Cell*, **17**, 351–365.
29. Deng, H.X., Shi, Y., Furukawa, Y., Zhai, H., Fu, R., Liu, E., Gorrie, G.H., Khan, M.S., Hung, W.Y., Bigio, E.H. *et al.* (2006) Conversion to the amyotrophic lateral sclerosis phenotype is associated with intermolecular linked insoluble aggregates of SOD1 in mitochondria. *Proc. Natl Acad. Sci. USA*, **103**, 7142–7147.
30. Wate, R., Takahashi, S., Ito, H., Kusaka, H., Kubota, Y., Suetomi, K., Sato, H. and Okayasu, R. (2005) Radio-sensitivity of the cells from amyotrophic lateral sclerosis model mice transfected with human mutant SOD1. *J. Radiat. Res. (Tokyo)*, **46**, 67–73.
31. Reaume, A.G., Elliott, J.L., Hoffman, E.K., Kowall, N.W., Ferrante, R.J., Siwek, D.F., Wilcox, H.M., Flood, D.G., Beal, M.F., Brown, R.H., Jr *et al.* (1996) Motor neurons in Cu/Zn superoxide dismutase-deficient mice develop normally but exhibit enhanced cell death after axonal injury. *Nat. Genet.*, **13**, 43–47.
32. Kondo, T., Reaume, A.G., Huang, T.T., Carlson, E., Murakami, K., Chen, S.F., Hoffman, E.K., Scott, R.W., Epstein, C.J. and Chan, P.H. (1997) Reduction of CuZn-superoxide dismutase activity exacerbates neuronal cell injury and edema formation after transient focal cerebral ischemia. *J. Neurosci.*, **17**, 4180–4189.
33. Huang, T.T., Yasunami, M., Carlson, E.J., Gillespie, A.M., Reaume, A.G., Hoffman, E.K., Chan, P.H., Scott, R.W. and Epstein, C.J. (1997) Superoxide-mediated cytotoxicity in superoxide dismutase-deficient fetal fibroblasts. *Arch. Biochem. Biophys.*, **344**, 424–432.
34. Shibata, N. (2001) Transgenic mouse model for familial amyotrophic lateral sclerosis with superoxide dismutase-1 mutation. *Neuropathology*, **21**, 82–92.
35. Liu, D., Bao, F., Wen, J. and Liu, J. (2007) Mutation of superoxide dismutase elevates reactive species: comparison of nitration and oxidation of proteins in different brain regions of transgenic mice with amyotrophic lateral sclerosis. *Neuroscience*, **145**, 255–264.
36. Takeuchi, H., Kobayashi, Y., Ishigaki, S., Doyu, M. and Sobue, G. (2002) Mitochondrial localization of mutant superoxide dismutase 1 triggers caspase-dependent cell death in a cellular model of familial amyotrophic lateral sclerosis. *J. Biol. Chem.*, **277**, 50966–50972.
37. Bruijn, L.I., Houseweart, M.K., Kato, S., Anderson, K.L., Anderson, S.D., Ohama, E., Reaume, A.G., Scott, R.W. and Cleveland, D.W. (1998) Aggregation and motor neuron toxicity of an ALS-linked SOD1 mutant independent from wild-type SOD1. *Science*, **281**, 1851–1854.
38. Ranganathan, S. and Bowser, R. (2003) Alterations in G1 to S phase cell-cycle regulators during amyotrophic lateral sclerosis. *Am. J. Pathol.*, **162**, 823–835.
39. Bowling, A.C., Barkowski, E.E., McKenna-Yasek, D., Sapp, P., Horvitz, H.R., Beal, M.F. and Brown, R.H., Jr (1995) Superoxide

dismutase concentration and activity in familial amyotrophic lateral sclerosis. *J. Neurochem.*, **64**, 2366–2369.
40. Kato, S., Saeki, Y., Aoki, M., Nagai, M., Ishigaki, A., Itoyama, Y., Kato, M., Asayama, K., Awaya, A., Hirano, A. *et al.* (2004) Histological evidence of redox system breakdown caused by superoxide dismutase 1 (SOD1) aggregation is common to SOD1-mutated motor neurons in humans and animal models. *Acta Neuropathol. (Berl)*, **107**, 149–158.
41. Tortarolo, M., Crossthwaite, A.J., Conforti, L., Spencer, J.P., Williams, R.J., Bendotti, C. and Rattray, M. (2004) Expression of SOD1 G93A or wild-type SOD1 in primary cultures of astrocytes down-regulates the glutamate transporter GLT-1: lack of involvement of oxidative stress. *J. Neurochem.*, **88**, 481–493.
42. Wen, W., Meinkoth, J.L., Tsien, R.Y. and Taylor, S.S. (1995) Identification of a signal for rapid export of proteins from the nucleus. *Cell*, **82**, 463–473.
43. Newmeyer, D.D. and Forbes, D.J. (1988) Nuclear import can be separated into distinct steps *in vitro*: nuclear pore binding and translocation. *Cell*, **52**, 641–653.
44. Riso, P., Pinder, A., Santangelo, A. and Porrini, M. (1999) Does tomato consumption effectively increase the resistance of lymphocyte DNA to oxidative damage? *Am. J. Clin. Nutr.*, **69**, 712–718.